Time-optimal performance of Josephson charge qubits: A process tomography approach

Robert Roloff* and Walter Pötz†

Fachbereich Theoretische Physik, Institut für Physik, Karl-Franzens Universität Graz, Universitätsplatz 5, 8010 Graz, Austria

(Received 9 February 2009; revised manuscript received 30 April 2009; published 15 June 2009)

A process tomography based optimization scheme for open quantum systems is used to determine the performance limits of Josephson charge qubits within current experimental means. The qubit is modeled microscopically as an open quantum system taking into account state leakage, as well as environment-induced dephasing based on experimental noise spectra. Within time-optimal control theory, we show that the competing requirements for suppression of state leakage and dephasing can be met by an external control of the effective qubit-environment interaction, yielding minimal gate fidelity losses of around $\Delta F \approx 10^{-3}$ under typical experimental conditions.

DOI: 10.1103/PhysRevB.79.224516 PACS number(s): 85.25.Cp, 03.67.Lx, 02.30.Yy, 03.67.Pp

I. INTRODUCTION

Within the circuit model of quantum computing, the fundamental building block of a quantum computer is the *quantum bit* or *qubit*. Our ability to precisely execute unitary operations within qubits is an essential prerequisite for the implementation of quantum algorithms and for harnessing the full computational power of a more complex quantum system. Among the various proposals for a physical realization of a qubit, specially designed superconducting circuits have been identified as promising candidates.[1,2] Their potential is mostly founded on the high technological standards by which superconducting quantum interference devices (SQUIDs) can be fabricated and controlled, as well as their promise regarding array scalability.[3] Several types of Josephson-junction-based qubit designs, such as charge, phase, and flux qubits, have been proposed and explored in the laboratory.[4–7] Conditional gate operations have already been performed experimentally.[8,9]

While preliminary results indeed look promising, considerable improvement in gate performance will be necessary to make these structures useful in larger arrays of quantum gates. Similar to all solid-state-based qubits, Josephson qubits suffer from two main shortcomings: they are quantum two-level systems only within approximation and there is non-negligible coupling to the environment. The former may result in leakage to noncomputational basis states which affects the fidelity of quantum gates.[10–14] The latter results in an unwanted population relaxation and destruction of state superpositions, both being detrimental for quantum computation.[15,16]

In this work we study Josephson charge qubits and show how the conflicting requirements for suppression of both state leakage and decoherence can be accomplished within optimal control theory. In the first part, we outline the model for the Josephson charge qubit, including leakage and environmental interaction on which we base our study. Then, we formulate a cost functional for state-independent optimization of open quantum systems based on the Kraus representation and process tomography. This method can be readily applied to any open quantum system, including other qubit implementations as well as multiqubit gates, and is not necessarily restricted to solid-state realizations. In the remainder of the paper, we demonstrate the approach for the Hadamard gate implementation.

II. JOSEPHSON CHARGE QUBIT

The basic structure of a Josephson charge qubit is shown in Fig. 1.[2,4,17] The characteristic energy scales are the charging energy E_C of the superconducting island, the Josephson coupling energy E_J^0, and the superconducting energy gap Δ. If Δ is the largest energy, the problem can be reduced to a situation where no quasiparticle excitation is found on the island and only Cooper pairs can tunnel through the Josephson junctions. Cooper-pair relaxation on the island, as well as quasiparticles tunneling from the reservoir onto the island, contributes, in principle, to relaxation and decoherence. The latter takes place at time scales of the order $(T_2^{\mathrm{qp}})^{-1} \sim \frac{g_T \delta_r}{2\pi\hbar} N_{\mathrm{qp}}$, where g_T denotes the conductance of the Josephson junctions (in units of e^2/h), δ_r is the quasiparticle level spacing in the reservoir, and N_{qp} is the number of quasiparticles.[18,19] For typical charge-qubit architectures, T_2^{qp} is of the order of 10^{-3}–10^{-5} s and, thus, on a time scale much larger than we are investigating in the present work. Cooper-pair relaxation within the island is even weaker and may be neglected too. Within the charge basis $\{|n\rangle\}$, the Hamiltonian of the system,

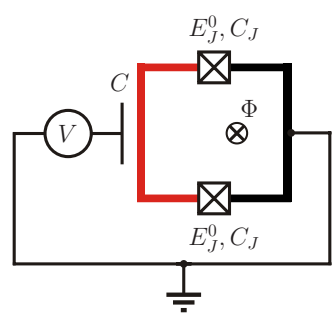

FIG. 1. (Color online) Superconducting charge qubit with two Josephson junctions. The two junctions are realized by small insulating layers which divide a superconducting ring into a small island (red/gray) and a reservoir (thick black) (Ref. 2). The qubit is driven by an external flux Φ and a gate voltage V. The voltage is coupled capacitively (C) to the island. The Josephson junctions are characterized by a capacitance C_J and the Josephson coupling energy E_J^0.

$$H_S = 4E_C[n - n_c(V)]^2 - 2E_J^0 \cos\left(\pi\frac{\Phi}{\Phi_0}\right)\cos\Theta, \quad (1)$$

may be written as

$$H_S = \sum_n \{4E_C[n - n_c(V)]^2|n\rangle\langle n| + E_J(\Phi)(|n+1\rangle\langle n| + |n\rangle\langle n+1|)\}, \quad (2)$$

with Θ (the phase difference across a Josephson junction) being the conjugate variable to the number n of additional Cooper pairs on the island,[2]

$$E_J(\Phi) = -E_J^0 \cos(\pi\Phi/\Phi_0) \quad (3)$$

and $n_c(V)=VC/(2e)$ contain two independent physical control fields, $V=V_g+V_p$ and Φ, where V_g and V_p denote a dc and a pulse gate voltage, respectively. Φ is the external magnetic flux. The latter can be used to tune $E_J(\Phi)$ between $-E_J^0$ and 0.[20] By proper choice of the dc gate voltage V_g, one can set the qubit "working point" to the charge degeneracy point, where the qubit is insensitive to charge fluctuations up to the first order. Using, next to the computational basis $\{|0\rangle,|1\rangle\}$, two adjacent leakage states $|-1\rangle$ and $|2\rangle$, the effective "leaky qubit" Hamiltonian at the charge degeneracy point reads

$$H_S = \begin{bmatrix} 8E_C & E_J(\Phi) & 0 & 0 \\ E_J(\Phi) & 0 & E_J(\Phi) & 0 \\ 0 & E_J(\Phi) & 0 & E_J(\Phi) \\ 0 & 0 & E_J(\Phi) & 8E_C \end{bmatrix} + 4E_C n_p(t)X,$$

$$X = \begin{bmatrix} 3 & 0 & 0 & 0 \\ 0 & 1 & 0 & 0 \\ 0 & 0 & -1 & 0 \\ 0 & 0 & 0 & -3 \end{bmatrix}, \quad n_p = n_p(V_p). \quad (4)$$

For our computation we consider a typical charge qubit with energies $E_C=150\ \mu$eV and $E_J^0=35\ \mu$eV from the experiment.[4,15,21] The qubit can be controlled by tuning the external magnetic flux $[\Phi=\Phi(t)]$ and the applied pulse gate voltage $[V_p=V_p(t)]$.

In the derivation of the Hamiltonian [Eq. (1)], the loop inductance of the superconducting ring has been neglected. For the parameters used in the present work, this approximation is justified if $L \ll \Phi_0^2/(4\pi^2 E_J^0) \approx 20$ nH. We also assume that the Josephson coupling energies of the two junctions are identical. However, if $E_J^0 \to E_J^0 + \delta E_J^0$ for one of the junctions, Eq. (3) turns into $E_J(\Phi) = -E_J^0|(1+\eta)\cos(\pi\frac{\Phi}{\Phi_0}) + i\eta\sin(\pi\frac{\Phi}{\Phi_0})|$, with $\eta \equiv \frac{\delta E_J^0}{2E_J^0}$, see, e.g., Ref. 20. In order to avoid such an asymmetry, it is possible to substitute one of the Josephson junctions in Fig. 1 by a SQUID, which enables one to tune the Josephson energies to be equal.[17]

In superconducting qubits the dominant dephasing mechanism (at low temperature) is attributed to noise which changes from $1/f$ to Ohmic behavior at frequencies of typically $k_BT/\hbar$.[15] The microscopic origin of the $1/f$ noise is not fully understood yet but it is believed that it originates from background charge fluctuations. Ohmic contributions may result from intrinsic sources or from gate lines.[15,16,21] We map these fluctuations onto a bath of harmonic oscillators coupling linearly to the qubit.[22,23] The system is thus modeled by a Hamiltonian of the form

$$H(t) = H_S(t) + H_B + H_I, \quad H_B = \sum_k \hbar\omega_k b_k^\dagger b_k,$$

$$H_I = \hbar X \otimes \sum_k g_k(b_k^\dagger + b_k) \equiv X \otimes \Gamma, \quad (5)$$

where g_k is the effective coupling constant of the spin-boson interaction and $b_k^\dagger$ and b_k are the bosonic creation and annihilation operators for the mode with frequency ω_k. The dynamics of the system, bosonic bath, and the interaction between the two, respectively, is governed by the Hamiltonians H_S, H_B, and H_I, whereby the external control field $\epsilon(t)$ to be optimized is contained in H_S only, thus assuming that there is no direct control over H_B and H_I.

Apart from correlation functions, noise has to be classified by its amplitude distribution (AD). For the spin-boson model with a thermal bath the AD is normal distributed (Gaussian noise), which agrees quite well with the experiment, especially at short time scales with which we are concerned.[24] Guided by the experimental results of Ref. 15, we construct the spectral density by choosing $J(\omega)=J_{1/f}(\omega)+J_f(\omega)$, consisting of a $1/f$ and an Ohmic contribution,[23]

$$J_{1/f} = \alpha_{1/f}/(4k_BT), \quad J_f(\omega) = \alpha_f/(2\hbar)\omega. \quad (6)$$

For thermal equilibrium, the noise spectrum $S_\Gamma(\omega)$ associated with the operator Γ in Eq. (5) in terms of $J(\omega)$ is then (a tilde denoting the interaction picture)

$$S_\Gamma(\omega) = \langle\{\tilde{\Gamma}(t),\tilde{\Gamma}(t')\}\rangle_\omega = \int_{-\infty}^{\infty} d\tau\{\tilde{\Gamma}(t),\tilde{\Gamma}(t')\}e^{i\tau\omega}$$

$$= 2\hbar J(\omega)\coth\left[\frac{\hbar\omega}{2k_BT}\right], \quad \tau \equiv t - t'. \quad (7)$$

For $\hbar\omega \ll 2k_BT$ and $\hbar\omega \gg 2k_BT$, Eqs. (6) and (7) give the $1/f$ noise spectrum, $S_{1/f}(\omega) \approx \alpha_{1/f}/\omega$, and the Ohmic spectrum, $S_\omega(\omega) \approx \alpha_f\omega$, respectively. The strength of the charge fluctuations (proportional to $\alpha_{1/f}$) has been determined in the experiment to saturate at $\sim(10^{-3}e)^2$ for temperatures lower than 200 mK.[24] The slope of the Ohmic contribution is given in Ref. 15. A plot of the specific noise spectrum which we use numerically can be seen in the inset of Fig. 3(a).

Inspection of Eqs. (4) reveals that simple control strategies for leakage suppression and minimization of decoherence are in conflict with one another. The most convenient way to minimize dephasing within the computational subspace would be a large absolute value of the Josephson coupling energy $E_J(\Phi)$ because it sets the minimum time (t_{op}) needed to perform unitary transformations which incorporate rotations around the x axis of the Bloch sphere (as needed for the Hadamard gate). The faster t_{op}, the lesser the effect of decoherence on the gate. However, in the present superconducting qubit architecture, $E_J(\Phi)$ is also responsible for coupling to the noncomputational basis states $|-1\rangle$ and $|2\rangle$. Due to the structure of X in Eq. (5), the net decoherence rate is enhanced when they participate in the dynamics. Thus, if

decoherence effects are present, the transfer of coherence to the leakage subspace is highly undesirable. In the unitary case, coherence can be transferred back to the computational subspace without loss (given sufficient control). These conflicting requirements, as well as the complexity of an open quantum system, make the design of pulses which maximize the fidelity of the quantum gate a nontrivial task.

III. STATE-INDEPENDENT OPTIMAL CONTROL

In the context of quantum information processing, coherent control of unitary operations within the qubit is of fundamental interest.[25] In contrast to the optimization of state-selective transitions, e.g., to maximize the probability of a certain pathway in a chemical reaction,[26] here we are interested in the optimization of the whole dynamical map. Hence, the qubit should perform a desired unitary operation, irrespective of its initial state. We call this task "state-independent" optimal control.

We consider a Hilbert space which is a tensor product of the Hilbert space of the open quantum system (from now on denoted as *system*) $\mathcal{H}_S$ and the Hilbert space of the environment (which we will call *bath*) $\mathcal{H}_B$, $\mathcal{H}=\mathcal{H}_S\otimes\mathcal{H}_B=(\mathcal{H}_{S1}\oplus\mathcal{H}_{S2})\otimes\mathcal{H}_B$. Within the system we distinguish between computational states on which the gate operation is specified, spanning $\mathcal{H}_{S1}$, and "leakage levels" spanning $\mathcal{H}_{S2}$.[27]

The task of state-independent optimization can be stated as follows. The density matrix of the system, $\rho_S(t)$, evolves in time according to the map, $\rho_S(0)\mapsto\rho_S(t)=\mathcal{E}_t\{\rho_S(0)\}$, for which the superoperator $\mathcal{E}_t$ is functionally dependent on externally applied control fields $\epsilon(t)$, i.e., $\mathcal{E}_t=\mathcal{E}_t[\epsilon]$. In order to maintain the positivity of $\rho_S(t)$, the map $\mathcal{E}$ has to be *completely positive* and, thus, can be represented by Kraus operators K_m,[28,29]

$$\rho_S(t)=\mathcal{E}_t[\epsilon]\{\rho_S(0)\}=\sum_m K_m[\epsilon](t)\rho_S(0)K_m^\dagger[\epsilon](t), \tag{8}$$

with $K_m[\epsilon](t)$ depending on the propagator of the composite system and, hence, on $\epsilon(t)$. We now want to find a control field $\epsilon^*(t)$ for which, at some final time t_f, $\mathcal{E}_{t_f}[\epsilon^*]$ approaches the desired mapping $\mathcal{E}_D$ as closely as possible. For quantum gate operations, for example, one would set

$$\mathcal{E}_D\{\,.\,\}=U_D(t_f)(\,.\,)U_D^\dagger(t_f), \tag{9}$$

where $U_D(t_f)$ is the unitary operation to be executed within the gate. In the context of quantum information theory it is useful to formulate a cost functional within the language of process tomography (see, e.g., Refs. 28 and 30–32) to define a measure of how well such a, not necessarily unitary, desired operation has been accomplished. We rewrite the mapping $\mathcal{E}$ by expanding the Kraus operators, $K_m(t)=\Sigma_n\alpha_{mn}\bar{K}_n$, with $\alpha_{mn}\in\mathbb{C}$ and $\bar{K}_n\in\mathcal{A}$, where $\mathcal{A}$ denotes a complete basis set of $M\times M$ matrices.[30] $M=M_C+M_L$ is the total number of orthonormal basis states, consisting of M_C computational and M_L leakage levels. The final state of the quantum system, starting out in $\rho(0)$, now reads

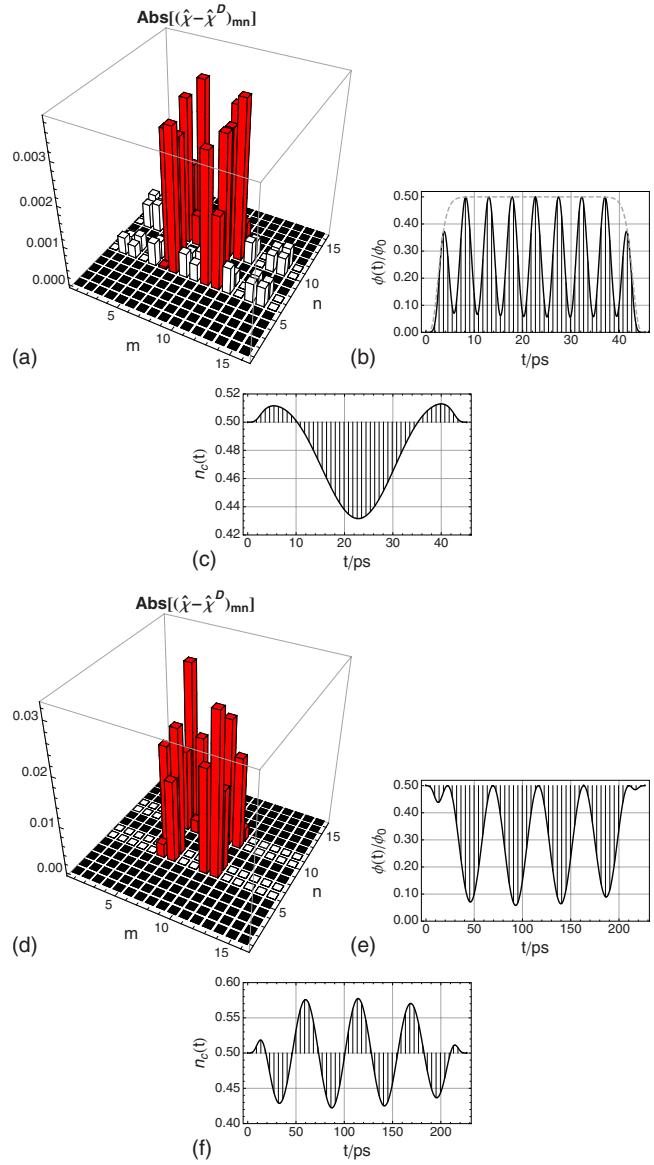

FIG. 2. (Color online) [(a) and (d)] Deviation of the Hadamard process tomography matrix elements $(\hat{\chi})_{mn}$ for optimized control fields [as given in Figs. 2(b), 2(c), 2(e), and 2(f)] from the desired values $(\hat{\chi}^D)_{mn}$. Black areas denote matrix elements which are irrelevant and, hence, arbitrary. They neither alter the qubit dynamics nor induce transitions out of the qubit subspace, i.e., leakage. For simplicity, they are plotted as zero [see also Eq. (17)]. Red (dark gray) columns show deviations of matrix elements which represent the gate operation within the qubit subspace, whereas white bars display leakage. [(b),(e) and (c),(f)] The strength of the optimal control fields lies within realistic values and the optimal solutions have a simple shape.

$$\rho(t_f)=\mathcal{E}_{t_f}\{\rho(0)\}=\sum_{m,n}\bar{K}_m\rho(0)\bar{K}_n^\dagger\chi_{mn}(t_f), \tag{10}$$

with $\chi_{mn}=\Sigma_k\alpha_{km}\alpha_{kn}^*$. For the example of the Josephson charge qubit described above, one has $M_C=2$, and $M_L=2$ with basis states $\{|0\rangle,|1\rangle\}$ and $\{|-1\rangle,|2\rangle\}$, respectively. Hence, we are dealing with a $M^2\times M^2=16\times 16$ representation of χ [see Figs. 2(a) and 2(d)]. The matrix χ in Eq. (10)

is usually termed *process tomography matrix* and in order to compute its elements, we choose a fixed set of operators $\{\sigma_j\}=\mathcal{B}$ (for simplicity we choose $\mathcal{B}=\mathcal{A}$) for which we determine the time evolution with respect to the mapping $\mathcal{E}$, i.e.,

$$\sigma_j(t_f) \equiv \mathcal{E}_{t_f}\{\sigma_j\}. \tag{11}$$

For one-qubit operations with two leakage levels or two-qubit gates, the tensor product of Pauli matrices $\tau_i \otimes \tau_j$ with $i,j \in \{x,y,z,0\}$ and $\tau_0=\mathbb{1}$ is a convenient choice for $\mathcal{A}$ and $\mathcal{B}$, which we use in present work. In the experiment, Eq. (11) corresponds to the preparation in and subsequent time evolution of suitable different initial states ($\sim\sigma_j$) of the quantum system. Recently, process tomography methods have been applied to superconducting qubits.[33,34] Because Eq. (8) is a linear mapping, one can rewrite Eq. (11) by

$$\mathcal{E}_{t_f}\{\sigma_j\} = \sum_k c_{jk}\sigma_k. \tag{12}$$

The mapping $\mathcal{E}_{t_f}$ is described completely in terms of coefficients c_{jk}, whose experimental determination involves quantum state tomography.[28] The last step in order to calculate the process tomography matrix relates c_{jk} to χ_{mn}. Therefore, we note that combining Eqs. (10)–(12),

$$\sum_k c_{jk}\sigma_k = \sum_{m,n} \sigma_m\sigma_j\sigma_n\chi_{mn}(t_f). \tag{13}$$

To extract the coefficients c_{jk} we apply the scalar product $\langle\sigma_i,\sigma_k\rangle=\delta_{ik}$ and get from Eqs. (11)–(13),

$$c_{ji} = \langle\sigma_i,\sigma_j(t_f)\rangle = \sum_{m,n}\langle\sigma_i,\sigma_m\sigma_j\sigma_n\rangle\chi_{mn}(t_f) \equiv \sum_{m,n} B_{imjn}\chi_{mn}(t_f). \tag{14}$$

$\chi_{mn}(t_f)$ can now be calculated by solving the system of linear equations $\langle\sigma_i,\sigma_j(t_f)\rangle=\Sigma_{m,n}B_{imjn}\chi_{mn}(t_f)$, which includes inversion of B.

Defining the operator[29]

$$\hat{\chi} = \sum_{m,n}(\bar{K}_n^* \otimes \bar{K}_m)\chi_{mn}, \tag{15}$$

we formulate a simple cost functional,

$$J \equiv \|P\hat{\chi} - \hat{\chi}^D\|^2 = \mathrm{tr}\{[P\hat{\chi} - \hat{\chi}^D][P\hat{\chi} - \hat{\chi}^D]^\dagger\}, \tag{16}$$

where P denotes the projector onto the M_C-dimensional computational Hilbert space and $0 \le J \le J_{max}=2M_C^2$. For the charge-qubit example,

$$P_{ij} = \sum_{k=6,7,10,11} \delta_{i,k}\delta_{j,k} \quad \text{with } i,j \in \{1,2,\ldots,M^2=16\}.$$

The transformation given in Eq. (15) corresponds to stacking the columns of the density matrix ρ_S from left to right on top of one another, i.e., $\rho_S \to \mathrm{col}(\rho_S)$, which yields a M^2-dimensional single-column vector, termed $\mathrm{col}(\rho_S)$. For the present work, this transformation is of the following form:

$$\rho_S = \begin{bmatrix} \rho_{11} & \rho_{12} & \rho_{13} & \rho_{14} \\ \rho_{21} & \boxed{\rho_{22}} & \boxed{\rho_{23}} & \rho_{24} \\ \rho_{31} & \boxed{\rho_{32}} & \boxed{\rho_{33}} & \rho_{34} \\ \rho_{41} & \rho_{42} & \rho_{43} & \rho_{44} \end{bmatrix} \to \mathrm{col}(\rho_S) = \begin{bmatrix} \rho_{11} \\ \rho_{21} \\ \rho_{31} \\ \rho_{41} \\ \rho_{12} \\ \boxed{\rho_{22}} \\ \boxed{\rho_{32}} \\ \rho_{42} \\ \rho_{13} \\ \boxed{\rho_{23}} \\ \boxed{\rho_{33}} \\ \rho_{43} \\ \rho_{14} \\ \rho_{24} \\ \rho_{34} \\ \rho_{44} \end{bmatrix}, \tag{17}$$

where the framed density-matrix elements belong to the computational subspace. The process tomography matrix χ changes accordingly, $\chi \to \hat{\chi}$, as given in Eq. (15). For further details see Ref. 29. J measures the norm distance between the target operation $\hat{\chi}^D$ and the actual operation $\hat{\chi}$ executed at time t_f for the control field ϵ. For the Hadamard gate with two leakage levels we set

$$\hat{\chi}^D = U_D^* \otimes U_D \quad \text{with} \quad U_D = \frac{1}{\sqrt{2}}\begin{bmatrix} 0 & 0 & 0 & 0 \\ 0 & 1 & 1 & 0 \\ 0 & 1 & -1 & 0 \\ 0 & 0 & 0 & 0 \end{bmatrix}.$$

A similar approach based on a superoperator formalism is given in Ref. 35.

IV. QUBIT DYNAMICS

Starting with the von Neumann equation for the full system dynamics, $\frac{d}{dt}\rho(t) = -\frac{i}{\hbar}[H(t),\rho(t)]$, the time evolution of the operators $\tilde{\sigma}_j(t)$ (with tilde denoting the interaction picture) is computed within a non-Markovian master equation in Born approximation,[36]

$$\frac{d}{dt}\tilde{\sigma}_j(t) = -\frac{1}{\hbar^2}\int_0^t dt'\ \mathrm{tr}_B\{[\tilde{H}_I(t),[\tilde{H}_I(t'),\tilde{\sigma}_j(t') \otimes \tilde{\rho}_B(0)]]\}, \tag{18}$$

using a numerical method described in Ref. 37 to deal with the kernel, which is nonlocal with respect to time. tr_B denotes the partial trace over all bosonic degrees of freedom. For $\tilde{\rho}_B(0)$ we assume a bath in thermal equilibrium at $T=50$ mK. We also introduce a sharp infrared and a continuous ultraviolet cutoff for the spectral density, i.e.,

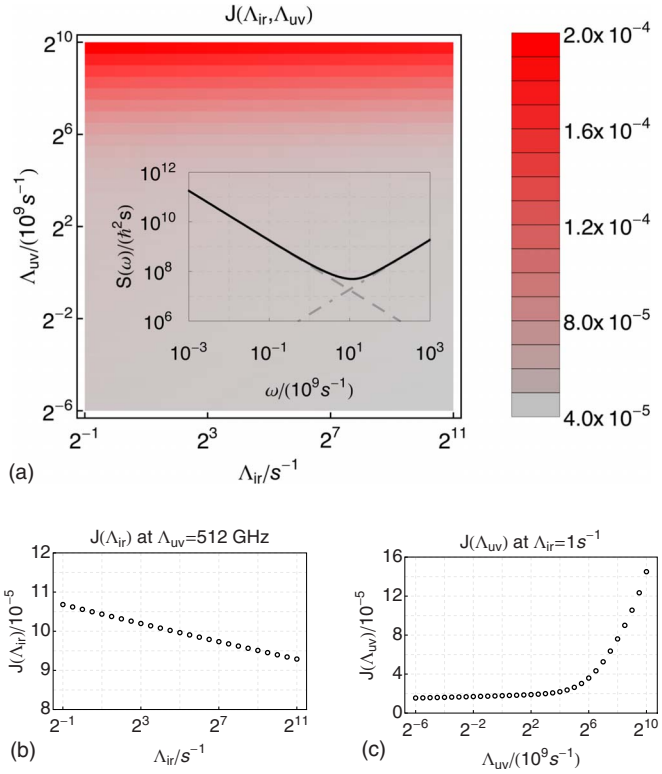

FIG. 3. (Color online) (a) Variation in the cost functional with respect to changes in the infrared and ultraviolet cutoff frequency. We used the pulse sequences shown in Figs. 2(b) and 2(c). Inset, solid line: noise spectrum employed for our calculations. Dashed and dotted-dashed lines represent $1/f$ and f noise contributions, respectively. (b) For a given ultraviolet cutoff, the cost functional shows a logarithmic dependence on $\Lambda_{\rm ir}$, i.e., $J(\Lambda_{\rm ir})\sim\log(1/\Lambda_{\rm ir})$, as expected (see Ref. 23). (c) For $J(\Lambda_{\rm uv})$ we obtain a logarithmic dependence over a broad regime. However, when Ohmic contributions become relevant the cost functional increases significantly.

$$J(\omega)\to[J_{1/f}(\omega)\Theta(\omega-\Lambda_{\rm ir})+J_f(\omega)]e^{-\omega/\Lambda_{\rm uv}}. \qquad (19)$$

We choose $\Lambda_{\rm ir}=2\pi\times 100$ Hz and $\Lambda_{\rm uv}=2\pi\times 100$ GHz (Ohmic noise in Josephson charge qubits has been measured up to frequencies of 100 GHz).[15] The lower bound for the infrared cutoff is determined by the data-acquisition time of the experiment. We have tested our optimal pulses with respect to different infrared and ultraviolet cutoff frequencies, see Figs. 3(a) and 3(b). When evaluating the trace of the double commutator in Eq. (18), one has to calculate bath correlation functions of the form

$$\langle\tilde{\Gamma}(t)\tilde{\Gamma}(t')\rangle=\mathrm{tr}_B\{\tilde{\Gamma}(t)\tilde{\Gamma}(t')\tilde{\rho}_B(0)\},$$

which can be derived analytically using the spectral density given in Eqs. (6) and (19).

V. RESULTS

Our strategy is to use short control pulses of high amplitude which move the qubit away from the degeneracy point only briefly and are within current experimental capabilities. We employ a time-optimal control strategy which incorporates the final time of the gate operation (t_f) as an additional control parameter, compatible with experimental control field strength. The control fields are of the form

$$n_c(t)=\frac{1}{2}+g(t)A_c\sin(\omega_c t+\varphi_c)e^{-\gamma_c(t-t_c^0)^2},$$

$$\frac{\Phi(t)}{\Phi_0}=g(t)\left\{1-\frac{A_\Phi}{2}[\{1+\sin(\omega_\Phi t+\varphi_\Phi)\}e^{-\gamma_\Phi(t-t_\Phi^0)^2}]\right\},$$

with $\{A_{c/\Phi},\omega_{c/\Phi},\varphi_{c/\Phi},\gamma_{c/\Phi},t_{c/\Phi}^0\}$ representing free parameters. Additionally, we restrict $\{n_c(t),\Phi(t)\}$ to start and end at the degeneracy point $(n_c=1/2,\Phi=0)$ by using an envelope function $g(t)$ [dashed gray line in Fig. 2(b)] and to satisfy other constraints imposed by the design of the superconducting circuit. There are other methods, such as driving the qubit by NMR-like techniques and adiabatic pulses, within which fidelities of $\sim$0.3–0.4 have been achieved.[38] Gate fidelities of $\sim$0.4 have also been reported for a CNOT gate implemented by two coupled flux qubits.[9] Recently, single qubit operations with gate errors of $1\sim 2\%$ have been realized within phase and transmon qubits.[34,39]

To optimize the cost functional Eq. (16) we use a parallelized constrained version of a differential evolution algorithm with 300 individuals per generation and 3000 generations per optimization run.[40] The algorithm finds an optimum for control fields given in Figs. 2(b) and 2(c). We typically choose crossing probabilities (C) and scaling parameters (S) within a range of $C\in[0.90,0.96]$ and $S\in[0.75,0.85]$. Variations in these parameters have a large impact on the convergence rate of the algorithm. All calculations have been performed on a 40 node SUN Linux Cluster.

For $t_f\approx 50$ ps, gate fidelity (F) losses $\Delta F=1-F\equiv(J[\epsilon^*]/J_{\max})^{1/2}$ as low as $\approx 10^{-3}$ are achievable. A plot of the associated matrix-element deviations from the Hadamard operation, $|(\hat{\chi}-\hat{\chi}^D)_{mn}|$, is shown in Fig. 2(a). Losses from decoherence (mainly included in red/dark gray bars) dominate over those from leakage (mainly included in white bars) by about a factor of 15, largely due to Ohmic contributions in the noise spectrum. To demonstrate the importance of including additional Cooper-pair occupation on the superconducting island within the model, we optimized the gate without leakage and then used these control fields to steer the qubit subjected to the leakage. The value of the cost functional increases by about 4 orders of magnitude corresponding to an increase in ΔF by 2 orders of magnitude. Incorporation of leakage states $|-2\rangle$ and $|3\rangle$ does not add significant fidelity losses for optimal pulses given in Figs. 2(a) and 2(b). Therefore, expanding the leakage state space beyond $|-1\rangle$ and $|2\rangle$ is not necessary.

We have also explored longer pulses ($t_f=200$ ps) and do not start at the degeneracy point with respect to Φ [the working point is now set at $(n_c=1/2,\Phi=\Phi_0/2)$, see Figs. 2(d)–2(f)]. These pulses show an enhanced reduction in leakage but they do lead to stronger decoherence because of an increased pulse duration. Also, moving the qubit working point away from the degeneracy point causes higher sensi-

tivity to fluctuations in the control fields. Typical fidelity losses ΔF for 200 ps pulses are about six times higher than those for the 50 ps ones ($\Delta F \approx 10^{-2}$).

Time-optimal control inevitably leads to short pulses (typically of the order of 50 ps for the present field intensities) whose generation in experiment is a demanding task. However, picosecond electrical pulses can be produced, e.g., by optoelectronic devices, such as photoconductive switches,[41] or by optical rectification of ultrashort optical pulses using nonlinear media (e.g., $LiTaO_3$).[42] Ultrafast pulse-shaping methods have been discussed extensively in Ref. 12.

VI. CONCLUSION

By applying a newly developed process tomography based optimal control theory for open quantum systems to a Josephson charge qubit, we have shown that one-qubit gates, such as the Hadamard gate, can be realized with remarkably high fidelity. The strategy has been to keep deviations of the control fields with respect to the degeneracy point as short as possible while performing the desired unitary operation in time-optimized fashion compatible with experimentally available control field strength. A fully quantum-mechanical description based on experimental noise spectra has been employed to model dephasing effects and additional noncomputational basis states have been included to account for unwanted Cooper-pair occupation on the superconducting island. Depending on the gate operation time, which has been treated as a variable, we could achieve fidelities of the order of $F \approx 1-10^{-3}$ to $1-10^{-2}$. In terms of the process tomography matrix this corresponds to errors of the order $\mathrm{Abs}[(\hat{\chi}-\hat{\chi}^D)_{mn}] \approx 10^{-3}-10^{-2}$. Thus we find that charge qubits can be made to perform at an equal level with current realizations of other Josephson qubits (such as phase, flux, or transmon qubits) which have been tested in experiment so far.

ACKNOWLEDGMENTS

The authors wish to acknowledge financial support of this work by FWF under Project No. P18829, as well as helpful discussions with M. Wenin.

*robert.roloff@uni-graz.at
†walter.poetz@uni-graz.at

[1] A. Shnirman, G. Schön, and Z. Hermon, Phys. Rev. Lett. **79**, 2371 (1997).
[2] Y. Makhlin, G. Schön, and A. Shnirman, Rev. Mod. Phys. **73**, 357 (2001).
[3] J. Q. You and F. Nori, Phys. Rev. B **68**, 064509 (2003).
[4] Y. Nakamura, Y. A. Pashkin, and J. S. Tsai, Nature (London) **398**, 786 (1999).
[5] J. M. Martinis, S. Nam, J. Aumentado, and C. Urbina, Phys. Rev. Lett. **89**, 117901 (2002).
[6] T. P. Orlando, J. E. Mooij, L. Tian, C. H. van der Wal, L. Levitov, S. Lloyd, and J. J. Mazo, Phys. Rev. B **60**, 15398 (1999).
[7] J. Clarke and F. K. Wilhelm, Nature (London) **453**, 1031 (2008).
[8] T. Yamamoto, Y. A. Pashkin, O. Astafiev, Y. Nakamura, and J. S. Tsai, Nature (London) **425**, 941 (2003).
[9] J. H. Plantenberg, P. C. de Groot, C. J. P. M. Harmans, and J. E. Mooij, Nature (London) **447**, 836 (2007).
[10] R. Fazio, G. M. Palma, and J. Siewert, Phys. Rev. Lett. **83**, 5385 (1999).
[11] S. Montangero, T. Calarco, and R. Fazio, Phys. Rev. Lett. **99**, 170501 (2007).
[12] A. Spörl, T. Schulte-Herbrüggen, S. J. Glaser, V. Bergholm, M. J. Storcz, J. Ferber, and F. K. Wilhelm, Phys. Rev. A **75**, 012302 (2007).
[13] P. Rebentrost and F. K. Wilhelm, Phys. Rev. B **79**, 060507(R) (2009).
[14] F. Motzoi, J. M. Gambetta, P. Rebentrost, and F. K. Wilhelm, arXiv:0901.0534 (unpublished).
[15] O. Astafiev, Y. A. Pashkin, Y. Nakamura, T. Yamamoto, and J. S. Tsai, Phys. Rev. Lett. **93**, 267007 (2004).
[16] G. Ithier *et al.*, Phys. Rev. B **72**, 134519 (2005).
[17] Y. Makhlin, G. Schön, and A. Shnirman, Nature (London) **398**, 305 (1999).
[18] R. Lutchyn, L. Glazman, and A. Larkin, Phys. Rev. B **72**, 014517 (2005).
[19] R. M. Lutchyn, L. I. Glazman, and A. I. Larkin, Phys. Rev. B **74**, 064515 (2006).
[20] A. Barone and G. Paternò, *Physics and Applications of the Josephson Effect* (Wiley, New York, 1982).
[21] Y. Nakamura, Y. A. Pashkin, T. Yamamoto, and J. S. Tsai, Phys. Rev. Lett. **88**, 047901 (2002).
[22] A. J. Leggett, S. Chakravarty, A. T. Dorsey, M. P. Fisher, A. Garg, and W. Zwerger, Rev. Mod. Phys. **59**, 1 (1987).
[23] Y. Makhlin, G. Schön, and A. Shnirman, J. Chem. Phys. **296**, 315 (2004).
[24] O. Astafiev, Y. A. Pashkin, Y. Nakamura, T. Yamamoto, and J. S. Tsai, Phys. Rev. Lett. **96**, 137001 (2006).
[25] J. P. Palao and R. Kosloff, Phys. Rev. Lett. **89**, 188301 (2002).
[26] D. J. Tannor and S. A. Rice, J. Chem. Phys. **83**, 5013 (1985).
[27] The difference between the tensor product and tensor sum structure with respect to optimization has been discussed in Ref. 43.
[28] M. Nielsen and I. Chuang, *Quantum Computation and Quantum Information* (Cambridge University Press, Cambridge, England, 2002).
[29] T. F. Havel, J. Math. Phys. **44**, 534 (2003).
[30] J. B. Altepeter, D. Branning, E. Jeffrey, T. C. Wei, P. G. Kwiat, R. T. Thew, J. L. O'Brien, M. A. Nielsen, and A. G. White, Phys. Rev. Lett. **90**, 193601 (2003).
[31] J. F. Poyatos, J. I. Cirac, and P. Zoller, Phys. Rev. Lett. **78**, 390 (1997).
[32] M. A. Nielsen, Phys. Lett. A **303**, 249 (2002).
[33] M. Neeley, M. Ansmann, R. C. Bialczak, M. Hofheinz, N. Katz, E. Lucero, A. O'Connell, H. Wang, A. N. Cleland, and J. M. Martinis, Nat. Phys. **4**, 523 (2008).
[34] J. M. Chow, J. M. Gambetta, L. Tornberg, J. Koch, L. S. Bishop, A. A. Houck, B. R. Johnson, L. Frunzio, S. M. Girvin, and R. J. Schoelkopf, Phys. Rev. Lett. **102**, 090502 (2009).
[35] M. Wenin and W. Pötz, Phys. Rev. B **78**, 165118 (2008).

[36] H. Carmichael, *Statistical Methods in Quantum Optics 1: Master Equations and Fokker-Planck Equations* (Springer, New York, 2002).
[37] M. Wenin and W. Pötz, Phys. Rev. A **74**, 022319 (2006).
[38] E. Collin, G. Ithier, A. Aassime, P. Joyez, D. Vion, and D. Esteve, Phys. Rev. Lett. **93**, 157005 (2004).
[39] E. Lucero, M. Hofheinz, M. Ansmann, R. C. Bialczak, N. Katz, M. Neeley, A. D. O'Connell, H. Wang, A. N. Cleland, and J. M. Martinis, Phys. Rev. Lett. **100**, 247001 (2008).
[40] http://www.icsi.berkeley.edu/storn/devcpp.zip
[41] J. F. Holzman, F. E. Vermeulen, and A. Y. Elezzabi, Appl. Phys. Lett. **76**, 134 (2000).
[42] A. Nahata and T. F. Heinz, Opt. Lett. **23**, 867 (1998).
[43] S. E. Sklarz and D. J. Tannor, J. Chem. Phys. **322**, 87 (2006).